[2]Kapania, R. K., Mohan, P., and Jakubowski, A., "Control of Thermal Deformations of Spherical Mirror Segment," *Journal of Spacecraft and Rockets*, Vol. 35, No. 2, 1998, pp. 156-162; also AIAA Paper 96-4145, 1996.

[3]Padula, S. L., and Palumbo, D. L., "Optimal Sensor/Actuator Locations for Active Structural Acoustic Control," AIAA Paper 98-1865, 1998.

[4]Chen, G. S., Bruno, R. J., and Salama, M., "Optimal Placement of Active/Passive Members in Truss Structures Using Simulated Annealing," *AIAA Journal*, Vol. 29, No. 8, 1991, pp. 1327–1334.

[5]Rao, S. S., Pan, T. S., and Venkayya, V. B., "Optimal Placement of Actuators in Actively Controlled Structures Using Genetic Algorithms," *AIAA Journal*, Vol. 29, No. 6, 1991, pp. 942, 943.

[6]Furuya, H., and Haftka, R. T., "Combining Genetic and Deterministic Algorithms for Locating Actuators on Space Structures," *Journal of Spacecraft and Rockets*, Vol. 33, No. 3, 1996, pp. 422–427.

[7]Sheng, L., and Kapania, R. K., "Genetic Algorithms for the Optimization of Piezoelectric Actuator Locations," AIAA Paper 2000-1581, April 2000.

[8]Kapania, R. K., and Mohan, P., "Static, Free Vibration and Thermal Analysis of Composite Plates and Shells Using a Flat Triangular Shell Element," *Computational Mechanics: An International Journal*, Vol. 17, No. 5, 1996, pp. 343–357.

[9]Goldberg, D. E., *Genetic Algorithms in Search, Optimization, and Machine Learning*, Addison Wesley Longman, Reading, MA, 1989.

[10]Holland, J. H., "Genetic Algorithms," *Scientific American*, July 1992, pp. 66–72.

[11]Mitchell, M., *An Introduction to Genetic Algorithms*, MIT Press, Cambridge, MA, 1996.

[12]Carroll, D. L., FORTRAN Genetic Algorithm Driver, URL: http://www.aic.nrl.navy.mil:80/galist/src/#fortran.

E. Livne
Associate Editor

Simultaneous Qualitative Health Monitoring and Adaptive Piezoelectric Sensoriactuation

Jeffrey S. Vipperman*
University of Pittsburgh, Pittsburgh, Pennsylvania 15261

Introduction

THERE is currently a large effort underway to efficiently and economically detect damage in structures such as aircraft, machines, bridges, and buildings. Historically, inspections have been conducted manually, which has typically resulted in downtime, labor costs, and human oversight. Whereas some forms of structural damage are fairly obvious on inspection, other forms are not. This is particularly true of fiber-reinforced polymer composites, which have become increasingly popular in their use through the years. Diagnostic tools have been developed to facilitate damage detection and notification. Various detection techniques have employed ultrasound, x-ray radiation, electrostatics, electromagnetics, acoustic emission, thermal imaging, fiber optics, strain sensing, and modal- or eigenanalysis.

There are pros and cons to each of these methods. These techniques typically require skilled human interaction to interpret the results of diagnostic tests and make some judgment as to whether structural damage is present or not. In the least, expert systems[1] or neural networks[2,3] are developed/trained to add autonomy to the detection process. For both of these methods, healthy as well as damaged structures must be observed to develop the systems. In addition, many methods are not very suitable (x rays and thermal imaging[4]) to in situ operation due to the shear bulk of the equipment, as well as expense. These limitations are overcome for ultrasound analysis by using portable hand-held units, or by using surface-bonded or embedded piezoelectric patches for ultrasonic actuation and sensing.[5–7] One paper has reported an analytical examination using interdigital electrodes on piezoceramics for ultrasonic sources and receivers.[8] Single patches can be used in a pulse/echo manner, or one patch can send sound through the structure while another receives.[7] Common to all of these approaches is using very short wavelength ultrasound acoustic waves to measure the distance to a reflective impedance discontinuity, resulting from a structural boundary or internal damage. Analyzing large structures with this method can be tedious. In addition, certain types of damage are difficult to detect with ultrasound, such as surface delaminations, because they are adjacent the natural boundary of the structure.

Embedded optical fibers have also been used to detect damage in composite materials. In one study a fiber optic nervous system was created throughout a structure.[9] When damage occurs, the optical fibers will break, disrupting the travel of light and indicating damage. A two-dimensional grid of fibers can be used to locate certain types of damage to within the resolution of the fiber optic array. Methods of strain sensing using fiber optics have also been employed for damage detection in composite materials at the expense of increased complexity.[10]

A tremendous amount of work has been done using system response measurements. These techniques are based on the observation that the modal properties (resonant frequencies and damping) of a structure will change with damage.[11] Some form of modeling is required to quantify the natural characteristics of the structure before and after damage. Good examples of such are the mass and stiffness matrices from finite element models,[11,12] transfer function parameters,[13] or analysis of the structural impulse response.[6,14] Many of these methods are model based and can require great computational effort, for example, to solve an eigenvalue problem.[11] The use of piezoelectric transducers has served to simplify the hardware requirements of these techniques[7] as well as preclude mass or stiffness loading in nondestructive evaluation methods.[7,14] These transducers are also used for acoustic emission evaluation.[15] It is known that, when a structure fails, a series of high-frequency stress pulses (acoustic emission) occur that can be monitored by specialized hardware to detect the onset of failure.

The proposed method is most similar to the previously reported technique of electromechanical impedance monitoring.[16,17] This method involves performing ultrasonic (frequency-domain) measurements of the coupled electromechanical impedance of a piezoelement attached to a host structure,[18] followed by data processing, which determines a scaler damage parameter.

Whereas this method does implicitly identify the capacitance and loss factor of the piezoceramic element, there are some significant differences from the technique presented hereinafter. Namely, the proposed method operates in a much lower bandwidth (sonic vs ultrasonic), directly measures a single scaler damage-related parameter in the time domain, and, thus, is somewhat simpler to implement, and functions simultaneously and autonomously of the collocated self-sensing transducer that is used to implement the device. The low-frequency operation of the proposed technique tends to delocalize the damage detection behavior reported by the impedance method,[17] possibly making the techniques complementary.

An example of the qualitative structural health monitoring capabilities of the adaptive piezoelectric sensoriactuator (APSA) is presented. The APSA provides a collocated sensor/actuator pair from a single piezoceramic patch and has been experimentally demonstrated for various control applications[19,20] and for piezoelectric transducer health monitoring.[21] Qualitative structural health monitoring capabilities are demonstrated using real-time monitoring of the piezoelectric permittivity, which is already implicitly measured by the adaptive piezoelectric sensoriactuator. The method is relatively simple, cheap, and easy to apply to existing structures; requires little computational effort; and does not interfere with the transduction capabilities of the APSA when used for active structural control systems or other applications.

Received 23 February 1999; revision received 24 October 2000; accepted for publication 6 April 2001.

*Assistant Professor, Department of Mechanical Engineering, 648 Benedum Engineering Hall. Member AIAA.

Theory

Piezoelectric Modeling

The four differential equations (three elastic and one electrical) that describe the behavior of a piezoelectric continuum can be written in tensor notation as[22,23]

$$c_{ijkl}u_{k,li} + e_{kij}\phi_{,ki} = \rho\ddot{u}_j \tag{1}$$

$$e_{kij}u_{i,jk} - \varepsilon_{ij}\phi_{,ij} = 0 \tag{2}$$

where c is the elastic stiffness, u is the displacement, e is a piezoelectric material constant, ϕ is the electric potential in volts, ρ is the material density, ε is the dielectric constant or permittivity, and $\ddot{(\,)}$ represents the second derivative with respect to time. For simplicity, the subscripts of the tensor notation are dropped in the text. Equations (1) and (2) represent a boundary value problem where the piezoelectric effect serves to couple the electric and elastic properties of the material. Typically, Eqs. (1) and (2) are solved for a particular absolute elastic and electric boundary condition such as free (zero stress) $(\,)^T$, clamped (zero strain) $(\,)^S$, constant field (short circuit) $(\,)^E$, or constant electrical displacement (charge) $(\,)^D$.

When operating bonded piezoceramic patches at low frequencies, the inertial effects can be ignored, and considering Eqs. (1) and (2) at constant electric field $(\,)^E$ and strain $(\,)^S$ results in the following familiar linear piezoelectric equations.

Sensor equation:

$$D_i = e_{ikl}S_{kl} + \varepsilon^S_{ik}E_j \tag{3}$$

Actuator equation:

$$T_{ij} = c^E_{ijkl}S_{kl} + e_{kij}E_k \tag{4}$$

where D is the electrical displacement (charge per area), S is the strain in the piezoelectric material, T is the stress the material, and E is the electric field (volts per meter). Note that the permittivity ε^S and stiffness c^E are taken at constant strain and constant field, respectively, because different boundary conditions would yield different values for these material constants.

Equation (3) represents the direct piezoelectric effect whereby a charge is produced when a material exhibiting piezoelectricity is mechanically strained. There are two terms in Eq. (3) that comprise the electric displacement: one due to the mechanical stress in the material, $e_{ikl}S_{kl}$, and one due to any externally applied electrical field, $\varepsilon^S_{ik}E_j$. The latter term results because piezoelectric materials typically have very high permittivity,[24] making them good capacitors. This electrical term is often referenced as an electrical feedthrough term because the input voltage field E feeds directly through to the output D, with the absence of dynamics. The physical interpretation of Eq. (4) (converse piezoelectric effect) is that any mechanical strain S_{ij} is again due to a mechanical, $c^E_{ijkl}S_{kl}$, and a piezoelectrical component, $e_{kij}E_k$. Note that the linear piezoelectric equations exhibit reciprocity[25] because they are both dependent on the same piezoelectric material constant e.

Bulk Dielectric Behavior

There is a well-known result that the dielectric constant of a piezoelectric material varies significantly depending on whether it is measured at zero strain e^S, that is, blocked, or zero stress e^T, that is, free.[22,23,26] The exact relationship between e^T and e^S is determined from the piezoelectric electromechanical coupling coefficient k, which is an indicator of efficiency in the electromechanical conversion that takes place within a piezoelectric material. This relationship is

$$\varepsilon^S = \varepsilon^T(1 - k^2) \tag{5}$$

Lead zirconate titanate (PZT) is the most widely used piezoceramic due to its excellent properties and performance. A PZT-5A material has $k = 0.7$, resulting in a difference of 50% between e^S and e^T, indicating that the elastic boundary conditions of this popular type of piezoelectric material can have a significant impact on its permittivity. The permittivity of the piezoceramic patch attached to the structure, ε^P, will be bounded by the free and blocked permittivities as $\varepsilon^P = [\varepsilon^S, \varepsilon^T]$.

The dielectric constant ε is related to the capacitance of the piezoceramic patch C_p by

$$C_p = \varepsilon A/t \tag{6}$$

where A is the area of the piezoceramic patch and t is the thickness of the patch, which also represents the separation distance between the two planar electroded faces. Because the capacitance C_p is linearly dependent on the permittivity of the piezoceramic, it will also vary in proportion to the elastic boundary conditions of the piezoelectric element.

When the same piezoelectric patch is used as an actuator and sensor (sensoriactuator), the electrical feedthrough term in Eq. (3) must be removed from the response.[19,21,27,28] When implemented, an analog electrical network with a reference capacitor and differencing circuit was still used, but now the gain was controlled by a digital signal processor, which uses a single coefficient adaptive filter.[19,29,30] This filter coefficient is directly proportional to the piezoceramic patch capacitance and, thus, the permittivity.[19,21] Hence, the APSA is readily amenable to monitoring piezoceramic permittivity in real time by monitoring this digital filter coefficient.

Adaptive Signal Processing

The least-mean-square (LMS) algorithm is chosen to adapt the internal gain of the adaptive piezoelectric sensoriactuator, due to its robustness and simplicity. A detailed analysis of the hybrid digital/analog compensation, including the convergence characteristics of the algorithm, can be found by Cole and Clark.[29] The LMS update equation for the single-filter coefficient $w(k)$ is

$$w(k+1) = w(k) - \mu e(k)x(k) \tag{7}$$

where μ is the learning rate parameter that controls convergence rate and the stability of the adaptive algorithm, k is the discrete time index, $e(k)$ is the output of the sensoriactuator electrical network that is the error signal to be minimized, and $x(k)$ is a low-level white noise signal used to train the APSA. One can show that a single coefficient is all that is necessary to remove the electrical feedthrough response, and further, the LMS algorithm converges to the optimal Wiener filter solution (see Ref. 29), which is proportional to the capacitance of the piezoelectric patch.[19]

Thus, by knowing the internal gains in the analog electrical network for the APSA, the piezoceramic capacitance can be computed and monitored in real time.[21] Damage to the structure will typically result in a minute, but detectable change in capacitance that can be automatically observed using a digital edge detector or discrete-time differentiator[21,31]:

$$y(k) = w(k) - w(k-1) \tag{8}$$

This simple filter, which is often used in image analysis, detects sudden changes in a discrete-time signal. By inspection of Eq. (8), it is observed that an output will only occur if the filter weight $w(k)$ changes. There will always be a low-level output because differentiation is an inherently noisy process. Thus, a threshold can be set that will distinguish between noise and any significant change in the filter weight, which would be an indication of the occurrence of damage in the piezoelectric transducer itself or of a change in structural stiffness as a result of damage. Decimation or skipping sample points[31] k can be used to monitor the capacitance change across different timescales.[21] Monitoring the piezoceramic transducer health itself has been demonstrated previously using this concept.[21] Also note that the health monitoring is independent of the sensoriactuator operation, enabling simultaneous active control and damage detection, if desired. In the next section, an experimental demonstration

of damage detection using these concepts and the adaptive piezoelectric sensoriactuator will be presented.

Experimental Results

A simple experiment was conducted to demonstrate the ability of the method to detect changes in boundary conditions, simulating, for example, a fastener failure in a structure. Capacitance values were measured for a beam piezostructure for both clamped–clamped and clamped–free boundary conditions. In addition, the boundary conditions were changed fairly quickly, allowing the resulting capacitance change to be measured in real time using the APSA. The beam is made of aluminum and measures $260 \times 38 \times 3$ mm in the clamped–clamped configuration and $280 \times 38 \times 3$ mm in the free–clamped configuration. A piezoceramic patch made of PZT-5A and measuring $53 \times 25 \times 0.19$ mm is attached to one face of the beam, as shown in Fig. 1. The APSA was implemented according to the literature,[19] except that strain conditioning[32] amplifiers were used as opposed to strain-rate conditioners. This change limited high-frequency noise in the circuitry.

The APSA was initiated and allowed to converge on the capacitance of the system in the clamped–clamped configuration. The capacitance determined by the APSA was recorded with a SIGLAB 2084 signal analyzer in real time as one end of the beam was unclamped. Figure 2a shows the resulting increase in capacitance as the clamp is removed at 500 s. Considering Eq. (5), one would expect the free end condition to result in higher capacitance, as observed. The slight settling of the capacitance over the following few minutes is the result of dielectric relaxation. Figure 2b shows the corresponding output of the edge detector, Eq. (8), which was optionally performed offline.

Note the spike that occurs at 500 s, which successfully indicates the change in capacitance. Again, the edge detector provides a level of autonomy to the operation of the device and could be used to trigger a warning alarm. Accordingly, the horizontal line marked

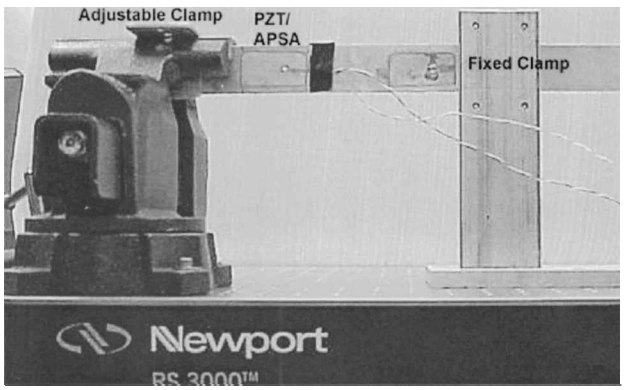

Fig. 1 Experimental beam with APSA attached.

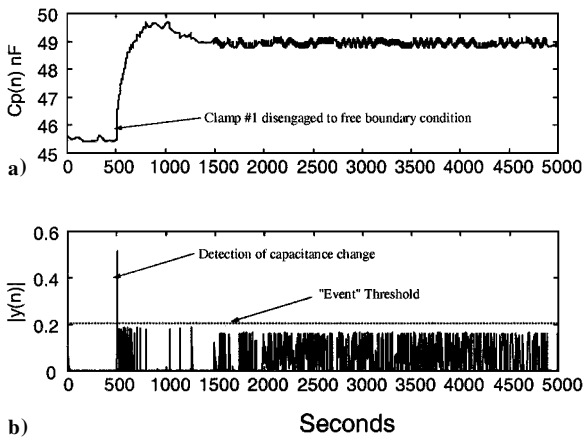

Fig. 2 Clamped–clamped to clamped–free boundary conditions.

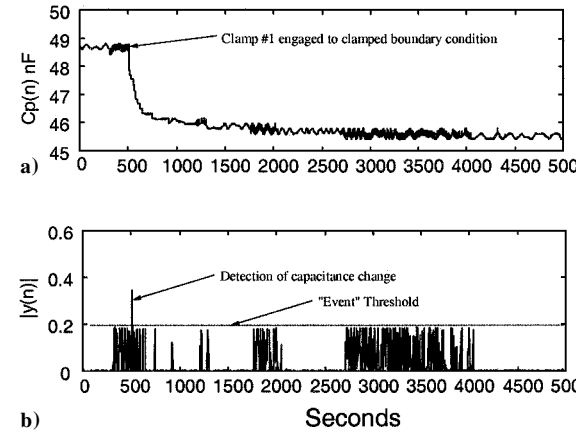

Fig. 3 Clamped–free back to clamped–clamped end conditions.

event threshold can be heuristically chosen for a particular setup. Also, decimation can be used to monitor simultaneously capacitance changes across multiple timescales, if desired.

The procedure associated with Figs. 2a and 2b was reversed, whereby the free end of the beam was quickly reclamped such that the beam was back to the original configuration. Figures 3a and 3b show the corresponding change in capacitance and edge-detector output. The capacitance now decreases, as expected, and converges to a value slightly higher than 45 nF, which was consistent with the original capacitance of the patch at the start of the demonstration.

Conclusions

A simple method of autonomous structural health monitoring is presented, which is based on real-time piezoelectric permittivity measurements using the adaptive piezoelectric sensoriactuator. Because the permittivity of a piezoelectric patch is dependent on the compliance of the attached structure, changes in stiffness or boundary conditions may be detected through changes in piezoelectric capacitance. A discrete-time differentiator or edge detector was used to automate the time-domain detection process. The concept was demonstrated through an experiment by quickly changing the boundary conditions of an aluminum beam piezostructure from clamped–free to clamped–clamped and back.

Future work will focus on analytically modeling and generalizing the permittivity dependence on structural stiffness and boundary conditions, as well as sensitivity of the technique to environmental factors. In addition, the ability to distinguish, quantify, and locate various types of damage with the method will be explored.

References

[1]Kwong, W. A., Passino, K. M., Laukonen, E. G., and Yurkovich, S., "Expert Supervision of Fuzzy Learning Systems for Fault Tolerant Aircraft Control," *Proceedings of IEEE*, Vol. 83, No. 3, 1995, pp. 466–483.

[2]Napolitano, M. R., Chen, C., and Naylo, S., "Aircraft Failure Detection and Identification Using Neural Networks," *Journal of Guidance, Control, and Dynamics*, Vol. 16, No. 6, 1993, pp. 999–1009.

[3]Islam, A. S., and Draig, K. C., "Damage Detection in Composite Structures Using Piezoelectric Materials," *Smart Materials and Structures*, Vol. 3, No. 3, 1994, pp. 318–328.

[4]Vikstrom, M., Backlund, J., and Olsson, K. A., "Nondestructive Testing of Sandwich Constructions Using Thermography," *Composite Structures*, Vol. 3, 1989, pp. 49–65.

[5]Crawley, E. F., and de Luis, J., "Use of Piezoelectric Actuators as Elements of Intelligent Structures," *AIAA Journal*, Vol. 25, No. 10, 1987, pp. 1373–1385.

[6]Luo, H., and Hanagud, S., "PVDF Sensor and Its Applications in Delamination Response Detection," *Proceedings of the AIAA/ASME/ASCE/AHS/ASC Structures, Structural Dynamics, and Materials Conference*, AIAA, Reston, VA, 1997, pp. 720–728.

[7]Smith, I. C., and Hoa, S. V., "Utilization of PVDF Sensors to Determine Impact Damage in Graphite/Epoxy Plates by Pcousto-Ultrasonic Technique," *Journal of Reinforced Plastics and Composites*, Vol. 13, No. 2, 1994, pp. 111–127.

[8]Moetakef, M. A., Joshi, S. P., and Lawrence, K. L., "Finite Element Simulation of Bulk Elastic Waves in Piezceramic Transducers Using Interdigital Electrodes," *Proceedings of the SPIE*, Vol. 2442, International Society of Optical Engineering, Bellingham, WA, 1995, pp. 182–187.

[9]Hofer, B., "Fibre Optic Damage Detection in Composite Structures," *Composites*, Vol. 17, No. 4, 1987, pp. 309–316.

[10]Waite, S. R., Tatam, R. P., and Jackson, A., "Use of Optical Fibre for Damage and Strain Detection in Composite Materials," *Composites*, Vol. 19, No. 6, 1988, pp. 435–442.

[11]Salawu, O. S., "Detection of Structural Damage Through Changes in Frequency: A Review," *Engineering Structures*, Vol. 19, No. 9, 1997, pp. 718–723.

[12]Tsai, W. H., and Yang, J. C. S., "Nondestructive Evaluations of Composite Structures Using System Identification Technique," *Journal of Engineering Materials and Technology*, Vol. 110, No. 2, 1988, pp. 134–139.

[13]Lew, J. S., "Using Transfer Parameter Changes for Damage Detection of Structures," *AIAA Journal*, Vol. 33, No. 11, 1995, pp. 2189–2193.

[14]Jian, X. H., Tzou, H. S., and Penn, L. S., "Damage Detection in by Piezoelectric Patches in a Free Vibration Method," *Journal of Composite Materials*, Vol. 31, No. 4, 1997, pp. 345–359.

[15]Valentin, D., and Busell, A. R., "Damage Detection in Carbon Fibre Epoxy Composites," *Composite Structures 2: Proceedings of 2nd International Conference*, Applied Science Publications, London, 1983, pp. 40–52.

[16]Sun, F. P., Chaudhry, Z., Liang, C., and Rogers, C. A., "Truss Structure Integrity Identification Using PZT Sensor–Actuator," *Journal of Intelligent Material Systems and Structures*, Vol. 6, No. 1, 1995, pp. 134–139.

[17]Ayres, J. W., Lalande, F., Chaudhry, Z., and Rogers, C. A., "Qualitative Impedance-Based Health Monitoring of Civil Infrastructures," *Smart Materials and Structures*, Vol. 7, No. 5, 1998, pp. 599–605.

[18]Liang, C., Sun, F. P., and Rogers, C. A., "Dynamic Analysis of Active Material Systems," *Journal of Vibration and Acoustics*, Vol. 116, No. 1, 1994, pp. 120–128.

[19]Vipperman, J. S., and Clark, R. L., "Implementation of an Adaptive Piezoelectric Sensoriactuator," *AIAA Journal*, Vol. 34, No. 10, 1996, pp. 2102–2109.

[20]Vipperman, J. S., and Clark, R. L., "Multivariable Feedback Active Structural Acoustic Control Using Piezoelectric Sensoriactuators," *Journal of the Acoustical Society of America*, Vol. 105, No. 1, 1999, pp. 219–225.

[21]Vipperman, J. S., and Clark, R. L., "Hybrid Analog and Digital Adaptive Compensation of Piezoelectric Sensoriactuators," *Proceedings of the AIAA/ASME/ASCE/AHS/ASC Structures, Structural Dynamics, and Materials Conference*, AIAA, Washington, DC, 1995, pp. 2854–2859.

[22]Board, I. S., *IEEE Standard on Piezoelectricity*, Inst. of Electrical and Electronics Engineers, New York, 1988, Sec. 2.

[23]Cady, W., *Piezoelectricity: An Introduction to the Theory and Applications of Electromechanical Phenomena in Crystals*, 2nd ed., Dover, New York, 1964, Chap. 8.

[24]Bunget, I., *Physics of Solid Dielectrics*, Elsevier, New York, 1984.

[25]Kinsler, L. E., Frey, A. R., Coppens, A. B., and Sanders, J. V., *Fundamentals of Acoustics*, 3rd ed., Wiley, New York, 1982.

[26]Jaffe, B., Cook, W., and Jaffe, H., *Piezoelectric Ceramics*, Academic Press, New York, 1971, Chap. 2.

[27]Dosch, J. J., Inman, D. J., and Garcia, E., "A Self-Sensing Piezoelectric Actuator for Collocated Control," *Journal of Intelligent Material Systems and Structures*, Vol. 3, Jan. 1992, pp. 166–185.

[28]Hagood, N. W., and Anderson, E. H., "Simultaneous Sensing and Actuation Using Piezoelectric Materials," *Active and Adaptive Optical Components*, SPIE Vol. 1453, International Society for Optical Engineering, Bellingham, WA, 1991, pp. 409–421.

[29]Cole, D. G., and Clark, R. L., "Adaptive Compensation of Piezoelectric Sensoriactuators," *Journal of Intelligent Material Systems and Structures*, Vol. 5, Sept. 1994, pp. 665–672.

[30]Vipperman, J. S., "Adaptive Piezoelectric Sensoriactuators for Active Structural Acoustic Control," Ph.D. Dissertation, Dept. of Mechanical Engineering, Duke Univ., Durham, NC, Feb. 1997.

[31]Oppenheim, A. V., and Schafer, R. W., *Digital Signal Processing*, Prentice–Hall, Englewood Cliffs, NJ, 1975.

[32]Vipperman, J. S., and Li, D., "Dielectric Response of Adaptive Piezoelectric Sensoriactuators," American Society of Mechanical Engineers, *International Mechanical Engineering Congress and Exposition Proceedings*, Nov. 2000.

A. M. Baz
Associate Editor

Experimental Validation of Nonlinear Shell Structural Dynamics

Daniel Berggren*
Royal Institute of Technology,
SE-100 44 Stockholm, Sweden

Introduction

In recent years there has been an increased interest in nonlinear aeroelasticity. Phenomena such as limit-cycle oscillations (LCOs) have been observed in flight testing,[1,2] but the cause of the LCOs is not yet fully understood. Most researchers agree that the limit cycles are an effect of nonlinearities in the fluid-structure interaction. However, it is not always obvious whether the dominant nonlinearities are caused by structural nonlinearities or aerodynamic nonlinearities.

Methods for analysis of LCOs have been developed by, for example, Patil et al.[3] and Tang et al.[4] with some success. The former models the wing using beam theory and the latter a method based on the von Kármán plate equations. The structural dynamic analysis can be improved using nonlinear shell finite elements for the wing. This is a well-established model[5,6] for structural dynamics analysis but has not yet been used much for analysis of nonlinear aeroelasticity.

The long term goal of the author's research is to investigate LCOs for a cantilever wing configuration using nonlinear shell finite elements combined with aerodynamic forces based on a linear unsteady potential flow model. However, there are not many test cases available in the open literature where experimental results are presented, making it possible to investigate the accuracy of the computational method. Because of this, experiments have been performed in the present study in order to investigate the accuracy of the structural dynamics model. In this Note a well-defined reference case is presented together with a brief description of the nonlinear analysis method used. The geometry, material properties, experimental results as well as computational results are given in order to make it possible to use the data as a reference case when developing methods for analysis of nonlinear structural dynamics.

Governing Equations

The equations of motion for a shell structure modeled with finite elements[7] are given by

$$\boldsymbol{M}\ddot{\boldsymbol{a}} + \boldsymbol{F}_{\text{int}}(\boldsymbol{a}) = \boldsymbol{F}_{\text{ext}}(t, \boldsymbol{a}) \tag{1}$$

where $\boldsymbol{M}$ is the linear mass matrix, $\boldsymbol{F}_{\text{int}}$ is a vector of internal forces, $\boldsymbol{F}_{\text{ext}}$ is a vector of external forces, and $\boldsymbol{a} = \boldsymbol{a}(t)$ is the time-dependent nodal displacement vector. The implicit Newmark average acceleration time-stepping algorithm[7] was chosen to solve Eq. (1) numerically. In each time step a Newton iteration has to be performed, and therefore, in addition to the internal forces, the tangential stiffness matrix of the structure has to be recomputed.

The shell element used here is similar to that developed by Parisch[8] and is based on a nonlinear displacement approach according to

$$\boldsymbol{u} = \boldsymbol{u}_m + \tfrac{1}{2}t\zeta[-\sin\varphi\,\hat{\boldsymbol{e}}_1 + \cos\varphi\sin\theta\,\hat{\boldsymbol{e}}_2 + (\cos\varphi\cos\theta - 1)\hat{\boldsymbol{e}}_3] \tag{2}$$

where $\boldsymbol{u}_m$ is the deformation of the midsurface and $\hat{\boldsymbol{e}}_1$ and $\hat{\boldsymbol{e}}_2$ are orthogonal unit vectors defined in the null space of the shell normal vector $\hat{\boldsymbol{e}}_3$. The normal of the element is assumed to undergo two consecutive rotations φ and θ. This formulation is exact for arbitrary translations and rotations of double curved shells in three

Received 7 February 2001; revision received 10 April 2001; accepted for publication 13 April 2001.

*Ph.D. Student, Department of Aeronautics.